Field testing of modular borehole monitoring with simultaneous distributed acoustic sensing and geophone vertical seismic profiles at Citronelle, Alabama

T.M. Daley[1]*, D.E. Miller[2], K. Dodds[3], P. Cook[1] and B.M. Freifeld[1]

[1]Lawrence Berkeley National Laboratory, 1 Cyclotron Road, Berkeley, California, USA, [2]Silixa Ltd, and [3]BP

∗E-mail: tmdaley@lbl.gov

ABSTRACT

A modular borehole monitoring concept has been implemented to provide a suite of well-based monitoring tools that can be deployed cost effectively in a flexible and robust package. The initial modular borehole monitoring system was deployed as part of a CO_2 injection test operated by the Southeast Regional Carbon Sequestration Partnership near Citronelle, Alabama. The Citronelle modular monitoring system transmits electrical power and signals, fibre-optic light pulses, and fluids between the surface and a reservoir. Additionally, a separate multi-conductor tubing-encapsulated line was used for borehole geophones, including a specialized clamp for casing clamping with tubing deployment. The deployment of geophones and fibre-optic cables allowed comparison testing of distributed acoustic sensing. We designed a large source effort (>64 sweeps per source point) to test fibre-optic vertical seismic profile and acquired data in 2013. The native measurement in the specific distributed acoustic sensing unit used (an iDAS from Silixa Ltd) is described as a localized strain rate. Following a processing flow of adaptive noise reduction and rebalancing the signal to dimensionless strain, improvement from repeated stacking of the source was observed. Conversion of the rebalanced strain signal to equivalent velocity units, via a scaling by local apparent velocity, allows quantitative comparison of distributed acoustic sensing and geophone data in units of velocity. We see a very good match of uncorrelated time series in both amplitude and phase, demonstrating that velocity-converted distributed acoustic sensing data can be analyzed equivalent to vertical geophones. We show that distributed acoustic sensing data, when averaged over an interval comparable to typical geophone spacing, can obtain signal-to-noise ratios of 18 dB to 24 dB below clamped geophones, a result that is variable with noise spectral amplitude because the noise characteristics are not identical. With vertical seismic profile processing, we demonstrate the effectiveness of downgoing deconvolution from the large spatial sampling of distributed acoustic sensing data, along with improved upgoing reflection quality. We conclude that the extra source effort currently needed for tubing-deployed distributed acoustic sensing vertical seismic profile, as part of a modular monitoring system, is well compensated by the extra spatial sampling and lower deployment cost as compared with conventional borehole geophones.

Key words: Acquisition, Borehole Geophysics, Seismics, Fibre-optic DAS

1 INTRODUCTION

Geologic storage of CO_2 is being widely studied for reduction in greenhouse gas emissions via carbon capture and storage (CCS) (e.g., IPCC 2005; CO2 Capture Project 2009). Subsurface monitoring is a key component of geologic carbon storage (GCS) (e.g., Freifeld *et al*. 2009). The overarching objective of monitoring GCS is to demonstrate the safe and effective long-term storage and integrity in the target reservoir. This is accomplished through a multi-faceted monitoring program by which the data acquired: (i) assure the public and regulators that the reservoir is behaving as intended, (ii) validate conceptual models developed for reservoir engineering and storage management, and (iii) demonstrate protection of drinking water and the greater environment. In the context of GCS, we have developed the modular borehole monitoring (MBM) concept to provide a suite of well-based monitoring tools that can be deployed cost effectively in a flexible and robust package at GCS sites (or other sites requiring dedicated monitoring wells) (Daley *et al*. 2013a, b). It incorporates many of the technologies considered most desirable for CO_2 plume characterization, such as pressure/temperature sensing, fluid sampling, and seismic monitoring, in a way that maximizes the data collected from a single wellbore. Fibre-optic cables were an early component of MBM design for CO_2 monitoring. One novel wellbore monitoring technology facilitated by the deployment of fibre-optic cable is distributed acoustic sensing (DAS), which allows seismic data acquisition without discrete sensors (Mateeva *et al*. 2012, 2014; Mestayer *et al*. 2012; Hartog *et al*. 2013; Miller *et al*. 2012). Following the initial proof-of-concept test of fibre-optic seismic acquisition with the Citronelle MBM system (Daley *et al*. 2013b), a test incorporating comparison of fibre-optic and geophone seismic data from vertical seismic profile (VSP) acquisition was accomplished. In this paper, we will describe the MBM system, its deployment for CO_2 monitoring at Citronelle, Alabama, the DAS processing flow leading to geophone equivalent data, and the results of our comparison of geophone and DAS VSP data.

2 BACKGROUND

The modular borehole monitoring (MBM) program was a three-year research and development program by Lawrence Berkeley National Laboratory and was commissioned by the CO2 Capture Project (www.co2captureproject.org) to develop a next-generation integrated well-based monitoring system for CO_2 sequestration. The MBM program was designed to identify a subset of critical technologies, perform the conceptual engineering design of an integrated monitoring platform, move the conceptual engineering design into detailed engineering and to design, fabricate, and install an MBM system. The initial MBM system was deployed as part of the Phase III Anthropogenic CO_2 Injection Field Test operated by the Southeast Regional Carbon Sequestration Partnership (SECARB 2012), in partnership with the U.S. Department of Energy. SECARB identified a series of thick, regionally extensive saline formations with high-quality seals within the U.S. Gulf

Coastal Region that have the potential to hold large volumes of CO_2. One such formation, i.e., the Cretaceous-age Paluxy Formation sandstone, is the target for the SECARB Anthropogenic CO_2 storage test. The anthropogenic CO_2 storage field test is being performed in southwest Alabama near the town of Citronelle in northern Mobile County (Fig. 1). The Paluxy Formation at the Citronelle Site is a fluvially deposited coarsening upward sequence of interbedded sands and shales that spans 2,865 m to 3,200 m deep (Esposito *et al*. 2011). The Paluxy is overlain by multiple geologic confining units that serve as vertical flow barriers to prevent CO_2 from escaping from the storage reservoir.

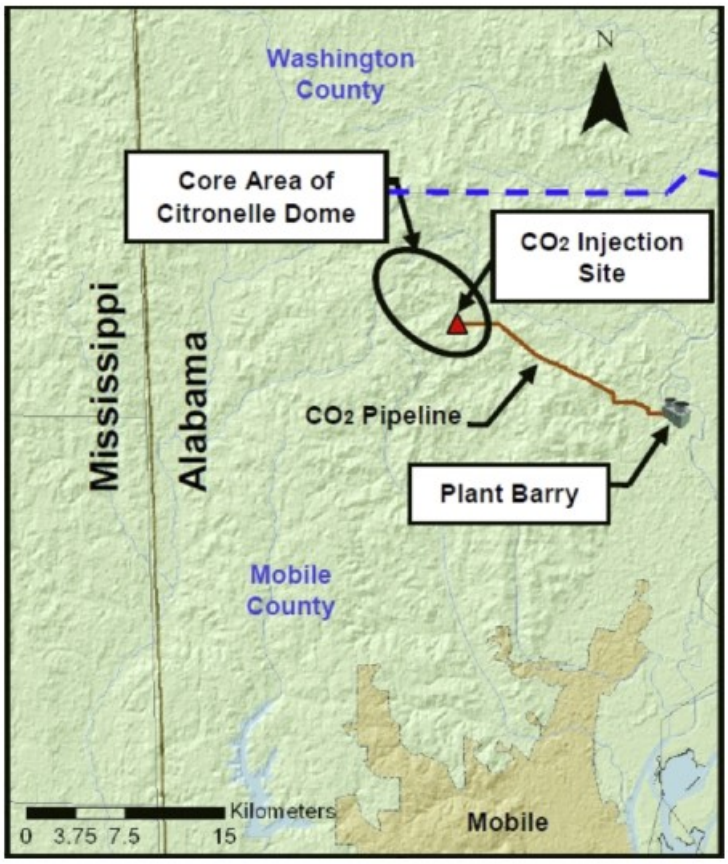

Figure 1 Location map showing Citronelle Dome, the injection site, Plant Barry (the CO_2 source site), and the nearby city of Mobile, Alabama, USA. From SECARB, 2012.

The CO_2 source for the test is a newly constructed 25-MW-equivalent post-combustion CO_2 capture facility at Alabama Power's existing 2,657-MW Barry Electric Generating Plant (Plant Barry). The CO_2 storage site is located within the Citronelle Dome geologic structure. The Citronelle Dome is expected to provide four-way closure free of faults or fracture zones and is located approximately 15 km west of Plant Barry. The primary target sand, referred to as “9460”, has porosity of 21.5% and permeability estimated at 450 mD (Riestenberg 2012). Temperatures at this depth are 108°C at a pressure of 298 bar.

3 MODULAR BOREHOLE MONITORING: FLATPACK DESIGN AND DEPLOYMENT AT CITRONELLE

The modular borehole monitoring (MBM) system deployed in the nearly vertical (33-m deviation over 3.58-km depth) Citronelle monitoring well D-9-8#2 included a ‘flatpack’ encapsulation of four stainless-steel lines containing the following: two tube-in-tube lines, a hybrid copper and fibre-optic cable, and a coaxial cable (Fig. 2). The flatpack utilized for the Citronelle MBM serves as the monitoring backbone, transmitting electrical power and signals, fibre-optic light pulses, and fluids from the surface to a reservoir. Additionally, a separate multi-conductor tubing-encapsulated conductor (TEC) line was used for borehole geophones (Fig. 2). The hybrid fibre-optic cable included two single-mode and two multi-mode fibres along with six copper conductors, and is used for temperature sensing and heat-pulse generation (Daley *et al*. 2013a). The tube-in-tube lines are used for geochemical sampling and hydraulic geophone clamps, whereas the coaxial line is used for digital transmission of multiple discrete, high-precision, pressure and temperature sensors. The location of individual sensors is flexible, whereas the deployment of the flatpack is standardized (Daley *et al*. 2013a). The instrument deployment for Citronelle is shown schematically in Fig. 3.

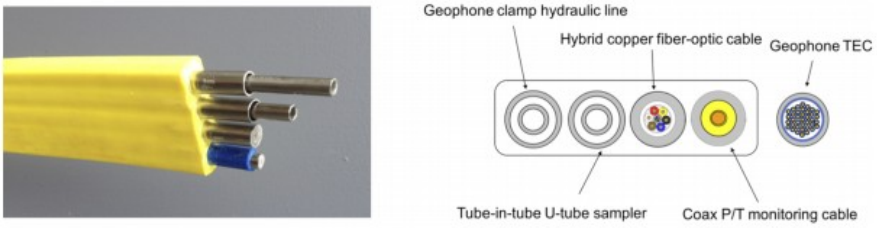

Figure 2 The MBM ‘flatpack’ (left) and the individual lines (right). Taken from (Daley *et al*. 2013b). The DAS data were recorded using one of the four fibres in the hybrid fibre-optic cable.

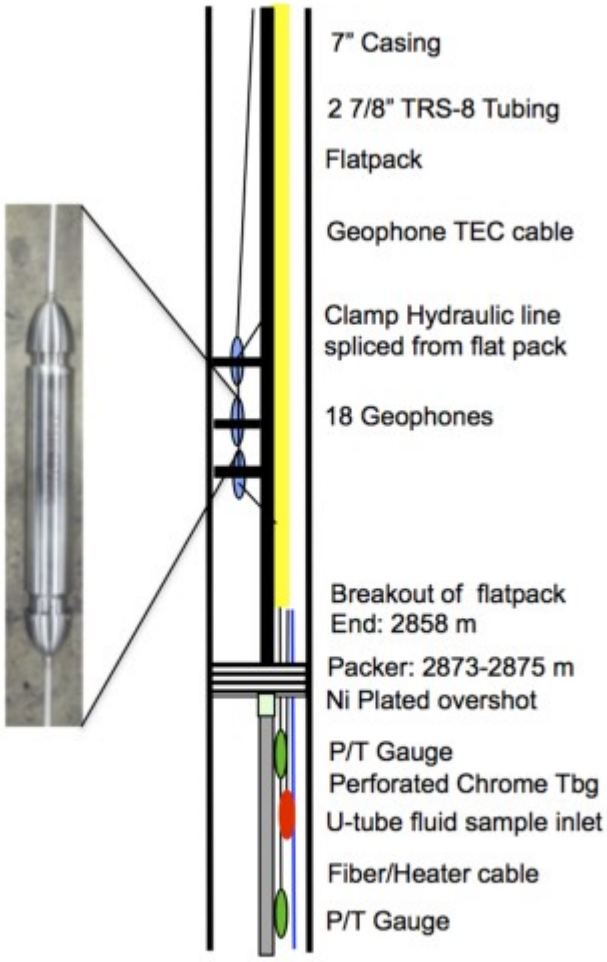

Figure 3 Schematic of MBM deployment at Citronelle (not to scale) with a photograph of the geophone with TEC cable (described in text).

Modular borehole monitoring geophone system design

The seismic system was designed for both active and passive monitoring. For passive monitoring, three-component sensors are required. For active monitoring, both three-component and one-component sensors are used. An initial design decision was the use of geophone sensors (other options considered were hydrophones and accelerometers). Hydrophones were considered because they are fluid coupled and therefore could be deployed in the fluid-filled annulus between tubing and casing without special clamping. Geophones were chosen based on cost, their capability of limiting tube-wave noise, and their use for passive monitoring. At the time of design, the option of distributed acoustic sensing (DAS) recording, as described in this paper, was not considered. There were 24 seismic data channels in the design (48 wires), used for 15 vertical geophones and three three-component geophones, giving a total of 18 geophone 'pods.' The three

components were placed at the top, bottom, and middle of the array. A spacing of 15.24 m (50 ft) was chosen between pods, which were externally identical for both the vertical and three-component geophones.

A key design decision was to use a geophone cable that was fully steel encased with no seals. Stainless-steel TEC cable was specified with 48 wires (24 geophones × 2 wire each), and the TEC was welded to each geophone pod. Previous deployments had failed at the connections between the cable and the pod or at downhole connections made to allow a packer to pass through. The use of a non-rotating packer overshot attachment, combined with welded connections between the geophone cable and pods, allowed removal of all seals and connectors from the seismic system. Figure 3 shows a single geophone pod welded to the TEC cable.

Modular borehole monitoring sensor clamping

The selection of geophones required that a clamping mechanism be used to provide coupling to the external formation, via the cemented casing. For the Citronelle MBM system, we designed a specialized clamp for tubing deployment (Fig. 4). The MBM clamp design attempts to decouple the conveyance tubing and the geophones mechanically so that the tubing mass has limited contact with the geophones once they are actively clamped. This is in addition to resolving the problem of casing contact during run-in. An active hydraulic setting mechanism is used, taking advantage of MBM control lines for hydraulic supply.

Figure 4 (left) MBM geophone with a hydraulic clamp, mounted on tubing with yellow flatpack. (right) Flatpack with a hydraulic line, each attached to tubing with steel banding. The DAS data were recorded using a fibre inside the flatpack, clamped to tubing as shown with clamps every ~10 m and banding every ~5 m.

The tubular design of the clamp support frame completely surrounds the deployment tubing with an annular and top and bottom gaps that allows the frame to float with full freedom around the tubing.

The MBM geophone clamp system is designed to lock itself mechanically. To gain mechanical advantage, a hydraulic actuator uses compound lever arms to multiply the clamping force. By design, an extended arm will not close on its own even if the hydraulic pressure is released. Therefore, after locking, the force is no longer dependent on the applied hydraulic pressure. The clamps therefore do not require sustained pressure or sealing of the hydraulic fluid system. The clamping force is about 500 kg (estimated from the designed clamp compression and a measured spring constant), whereas each sensor pod and clamp unit together weigh 18 kg.

After locking, release is allowed when the MBM system is pulled from the hole. The clamps are adjustable for planned tubing and casing diameters.

Other important design details of the MBM clamp system allow for both the geophone cable and the flatpack to pass by each geophone pod without interfering with the full floating design and while also providing protection to those components. The tube-in-tube hydraulic line is a closed-loop system so that it could be completely purged of air when pressured with hydraulic fluid.

Importantly, the fibre used for DAS, inside the flatpack, was clamped to the tubing (Fig. 4), and the tubing had point contact to the casing via cable clamp ‘protectors’ (not shown). Thus, the DAS fibre has a combination of fluid coupling and point mechanical coupling to the casing; therefore, there is greater uncertainty in the coupling to the casing and formation than with only point contact. At intervals in the well, the regularly spaced tubing clamps will be forced against casing, providing a variable mechanical coupling of flatpack to casing, whereas in between, there is fluid coupling between fibre/flatpack and casing/formation.

Initial seismic acquisition: geophone and fibre-optic vertical seismic profile

For geophone vertical seismic profile (VSP) analysis, we use the vertical components of the geophone array. Since DAS systems are sensitive to axial strain (as described below), a vertical geophone is the proper comparison to a vertical fibre cable. The initial MBM-VSP survey was planned as a baseline before CO_2 injection and included offset VSP source locations and a walkaway source line, both run with parameters designed for geophone recording.

As part of this testing, we utilized one of the single-mode fibres in the hybrid optical cable (Fig. 2), for DAS using a recorder provided by Silixa, Ltd (the iDAS recorder, Farhadiroushan *et al*. 2009). The Silixa iDAS system enables repeated measurement of dynamic strain distribution along a contiguous length of optical fibre. A laser pulse (of selectable width) is launched into the fibre, and a portion of light is scattered back and returns to the DAS

interrogator. Further discussion of the DAS signal processing is provided in following sections.

This test, conducted in March 2012, is described in (Daley *et al*. 2013b), where we found that seismic energy could be observed using the fibre in the MBM flatpack. However, body waves were observed only in the upper ~1 km of the well and the data had poor signal-to-noise ratio. Furthermore, issues related to the vibroseis source electronics led to uncertainty in the sweep parameters used (e.g., beginning and ending frequencies of the sweep).

Despite the limitations of the initial 2012 test, the results demonstrated that DAS data could be acquired with the MBM packaged fibres at Citronelle. Because of the sweep parameter uncertainty and the limited number of sweeps used (four to six per source point), we felt confident that significantly better DAS results could be obtained with acquisition dedicated to DAS recording.

4 VERTICAL SEISMIC PROFILE ACQUISITION FOR DISTRIBUTED ACOUSTIC SENSING AND GEOPHONES

A second test was designed with the goal of acquiring useful distributed acoustic sensing (DAS) data and determining the source effort (number of sweeps) needed to obtain signal-to-noise ratios comparable to those obtained with the modular borehole monitoring (MBM) geophone data.

Based on results from the initial DAS survey, we designed a large source effort (64 sweeps per source point rather than the previous 4) at a limited number of locations (maximum of 4). The data acquisition was conducted in August 2013.

The primary focus for testing was on source location (SP) 2021 (Fig. 5), which showed better data quality in the 2012 test (Daley *et al*. 2013b). Two other source locations were also used in DAS recording, as shown in Fig. 5; however, they are not discussed here.

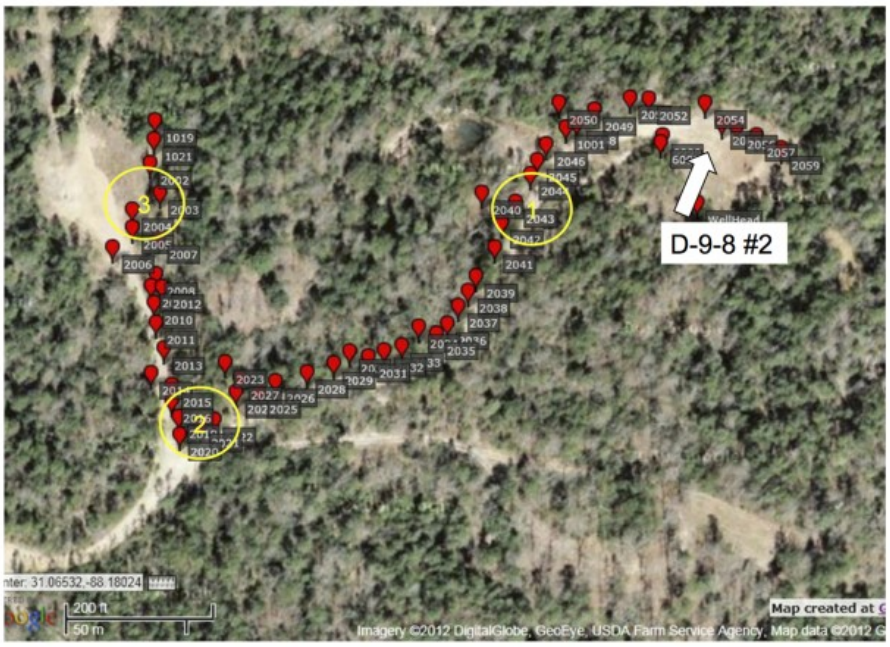

Figure 5 Location map of Citronelle MBM DAS testing. The MBM well, D-9-8 #2, is labelled with an arrow. Shot points for VSP are shown in red, with three DAS test focus points shown in yellow labels 1, 2, and 3. SP 2021 was the primary source location (yellow circled 2) with an offset of about 250 m (a near-zero offset for the geophones at about 2-km depth).

The maximum number of sweeps at each SP was determined in the field, based on near real-time analysis of stacked data. In the 2012 test (Daley *et al*. 2013b), real-time analysis was not possible because the iDAS was operated in continuous recording mode, with GPS timing used to 'cut' the vibroseis data out of the continuous records in post-processing. For the 2013 survey the iDAS system had a triggering box, and the vibroseis source electronics provided a +5 V, 20-ms width TTL pulse trigger to the Silixa iDAS system for zero time. GPS timing was also used for source and DAS systems as a check on timing. For best performance, the iDAS system recorded at a sample rate higher than the output geophysical records (10-kHz iDAS sampling for 1-kHz output data).

The vibroseis sweep used throughout was linear, 12 Hz to 110 Hz, and 16 s long with taper. The MBM geophone data were recorded on a DAQlink III recording system, made by Seismic Source.

The iDAS data acquired included testing of iDAS settings, requiring 280 total sweeps at SP 2021, of which 64 have settings used for analysis and reported on here. Additionally, 129 sweeps were acquired at SP 2003 and 64 sweeps at SPs 2040 and 2041 combined. Because of the number of sweeps recorded at each SP, the vibroseis truck had to move slightly to prevent road damage or coupling issues from too deep of a 'footprint' from the vibrator baseplate in the dirt/gravel road. The vibe moved up one pad width (about 1.5 m) for each set of 20 or 24 sweeps, making a 3 × 1 grid at each SP for each set of up to 64 sweeps.

5 DISTRIBUTED ACOUSTIC SENSING PROCESSING

Intelligent distributed acoustic sensor (iDAS) properties

Data acquired using distributed sensors is fundamentally different from data acquired using point sensors such as geophones, and the processing and analysis of such data potentially can benefit from being treated differently. Upon detailed study of the Citronelle data set, we realized that the experiment goal stated above, to compare source effort needed for comparable signal-to-noise ratios (SNRs) for distributed acoustic sensing (DAS) and geophones, is not the same as comparing two types of point sensors. Furthermore, since the physical property measured by a DAS system is different from the property measured by a geophone, the properties of the 'noise' in the SNR are also different for DAS and geophones.

Most borehole seismic tools currently are constructed using geophones (sensors of electric current generated by the motion of a coil in a magnetic field) that are idealized as sensitive to components of the local particle velocity of the medium at the point where the tool is clamped. The iDAS interrogator uses optical backscattering to monitor, in a moving window, the difference in optical path length changes between two sections of the fibre that are separated by a length *dz*, which is the 'gauge length.' To good approximation, change in this DAS response is linearly proportional to change in the average fibre elongation over the gauge length (Parker *et al*. 2014). The iDAS optical signal processing is designed to extract, for each channel and each successive optical pulse, the change in strain with respect to the previous pulse at the same channel.

In the iDAS native output format (as recorded at Citronelle), each digital sample is indexed by the centre location of a moving window along a cable's fibre core (the sample's 'channel', *z*) and recording time (the sample's 'time', *t*). Thus, if *u(z,t)* represents the dynamic displacement of the fibre at axial location *z* and time *t*, the iDAS output is an estimate of

$$\left[u\left(z+\frac{dz}{2},t+dt\right)-u\left(z-\frac{dz}{2},t+dt\right)\right] - \left[u\left(z+\frac{dz}{2},t\right)-u\left(z-\frac{dz}{2},t\right)\right], \quad (1)$$

where *dz* and *dt* are the reference spatial gauge distance and temporal sample interval, respectively. As such, the iDAS output can be equivalently regarded either as an estimate of the fibre strain rate

$$\frac{\partial}{\partial t}\left(\frac{\partial u}{\partial z}\right), \quad (2)$$

or as an estimate of the spatial derivative of fibre dynamic displacement

$$\frac{\partial}{\partial z}\left(\frac{\partial u}{\partial t}\right), \quad (3)$$

as calculated by difference operators applied in time or axial distance, respectively.

We can obtain a measurement of strain from the iDAS native strain rate since integration with respect to time converts strain rate to strain (typically followed by a suitable temporal bandpass filter). Moreover, for a propagating signal, integration with respect to distance is equivalent to integration with respect to time followed by multiplication by the propagation speed.

In the Citronelle survey, the gauge length was 10 m, and the channels were sampled every 2 m. Furthermore, the optical pulse rate was 10 kHz, thus producing a 2D output at 10 samples/ms and 0.5 samples/m. We refer to the operators on the channel dimension as “spatial,” whereas operators on the dimension sampled by successive optical pulses will be referred to as “temporal.”

Signal and noise

When comparing signal and noise for data recorded by the iDAS unit, the usable signal captured from the native output is typically limited by broadband noise that is inherent in the optical scattering process upon which the system depends. Because the system response is linear and coherent in dynamic local strain, repeated stacking of iDAS traces over repeated shots is expected to result in an SNR improvement following the inverse square root relationship between SNR and number of stacks. However, different from geophone sensors, analysis of the DAS optical scattering has shown that simple stacking is far from optimal in recovering weak signal in the presence of this noise.

It is well-known (e.g., Embree 1968; Widrow *et al*. 1975) that under the assumption that data consists of a set of measurements of common signal plus uncorrelated noise with known noise power, a weighted-mean stack can have significantly higher SNR than a simple mean stack, and that the optimal weights are inversely proportional to the noise power. In practice, this reduces the problem of determining optimal stacking weights to the problem of estimating noise power. Exploiting knowledge of the iDAS scattering processes and the opto-acoustic demodulation carried out within the iDAS, Silixa has developed a proprietary method to track the noise power and thereby accomplish the optimal stacking. As discussed above, the optimally weighted average (termed an adaptive stack) can be converted from strain rate to strain by a temporal operator (a band-limited integration in time, termed spectral rebalancing).

Figure 6 shows the result of applying this rebalanced adaptive stacking (followed by correlation with the sweep) for a representative subset of the Citronelle data and compares it with the result of simple stack and correlate processing. The SNR gain shown in Fig. 6 is 6.8 dB (from 13.9 dB to 20.7 dB) as calculated by normalizing the data by the peak signal, calculating RMS noise in the interval of 200 ms – 700 ms and averaging over the depth

interval of 2,000 m– 2,800 m. Further description of the adaptive rebalancing process is provided in Appendix.

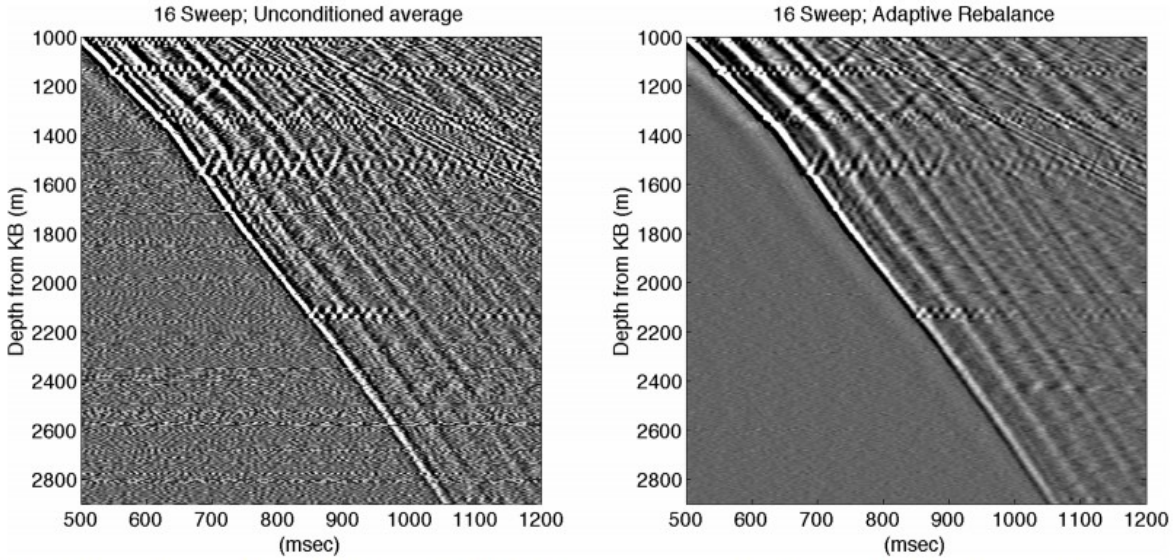

Figure 6 A randomly selected set of 16 DAS sweeps for SP 2021, comparing (left) stacking of native DAS data with (right) DAS data with adaptive stacking and spectral rebalancing.

Figure 7 compares this rebalanced result with data from the 2012 survey (and processing) at the same location. The data quality in Fig. 7 is greatly improved from the 2012 DAS acquisition shown in the inset (and in Daley *et al*. 2013b). In addition to the rebalancing operator, the new data benefitted from certainty of triggering, verified sweep parameters with a narrower frequency range, increased number of stacks (16 versus 4) and a newer, improved iDAS recording system.

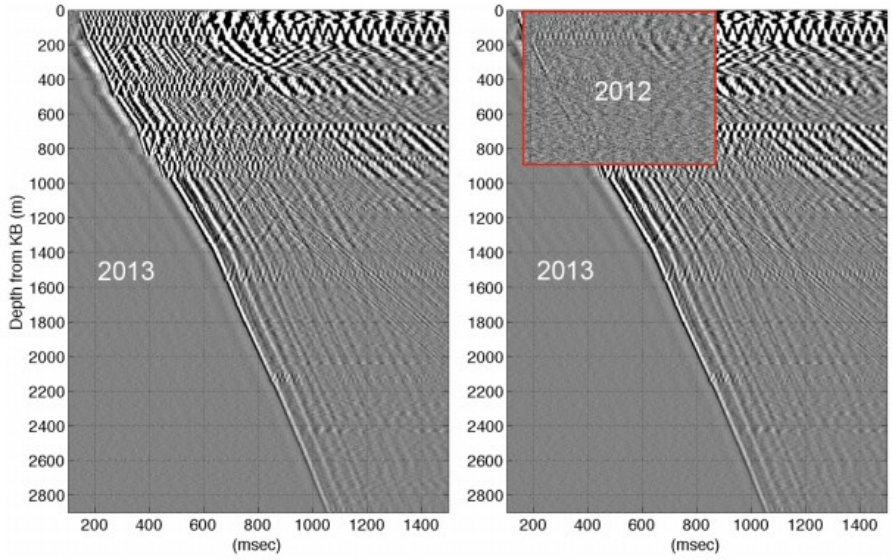

Figure 7 Correlated DAS data for SP 2021, comparing a four-sweep stack from the April 2012 survey (right inset) with a 16-sweep optimized stack from the August 2013 survey (left).

Conversion to geophone equivalent signal

An important issue for the use of the DAS is the relative response to industry ‘standard’ geophones. The MBM deployment provides a platform for direct comparison, with caveats for the clamping difference described above and the fundamental difference of distributed and point sensors. Since the rebalanced DAS recording is a local strain, comparison to a geophone (which measures particle velocity at a fixed point) requires conversion from strain to particle velocity, which we describe here.

First, consider propagating seismic signals, such as a harmonic plane wave. Strain, displacement, and particle velocity are related as follows (e.g., Aki and Richards 2002). For ε_{zz} = extensional strain in the z-direction, and u_z = displacement in the z-direction with velocity c, where $u_z = U\, e^{-i\omega\ (t-z/c)}$ and $v_z = du_z/dt = U\,(-i\omega)\, e^{-i\omega\ (t-z/c)}$ is the axial particle velocity, it follows that $\varepsilon_{zz} = du_z/dz = v_z/c$.

However, the relationship is more general and applies to any propagating disturbance with a stable phase function. Again writing $u(z,t)$ for the dynamic fibre displacement, a stably coupled propagating disturbance will be self-similar under suitable translation in space and time. That is, it will take the form $u(z,t) = u(\varphi)$ where $\varphi = (t_0 + t \pm z/c)$ is a characteristic phase function with propagation speed c. Differentiating with respect to time and distance respectively, we obtain the fibre particle velocity

$$v = \frac{\partial u}{\partial t} = \frac{\partial u}{\partial \varphi}, \quad (4)$$

and the fibre strain

$$\varepsilon = \frac{\partial u}{\partial z} = \pm \frac{1}{c} \frac{\partial u}{\partial \varphi}. \quad (5)$$

When we compare these equations, it is evident that $c\,\varepsilon = \pm v$. That is, the ratio between fibre particle velocity and fibre strain is given by the propagation speed along the fibre cable (apparent velocity) with a sign determined by direction of propagation. In general, the total fibre displacement, velocity, and strain may be the superposition of multiple events, and the propagation may be dispersive (i.e., propagation speed may depend on temporal frequency).

In situ coupling of the fibre cable to waves propagating in the Earth is also an important factor that can affect scaling DAS data to Earth's movement. It is beyond the scope of this paper to investigate the details of how to combine plane-wave decomposition and models of mechanical coupling to rescale data from complex fibre installations. In our case, the data appear to be consistent with the simple assumption that the fibre strain and the geophone output velocity are faithful transducers of the corresponding environmental strain and velocity. With this assumption, the rebalanced DAS signal is converted to equivalent geophone signal by multiplying the dimensionless strain by the local propagation speed (as determined from VSP moveout

data). In our VSP data, the vertical propagation speed across the zone covered by the geophones (1,829 m to 2,088 m) is approximately 3,500 m/s. We have used that value to rescale our noise-reduced, rebalanced iDAS strain values to velocity units for the uncorrelated data.

Following this velocity conversion, the Citronelle DAS data and SNR can be directly compared with the Citronelle geophone data. Figure 8 shows the uncorrelated DAS–geophone comparison. Correlated data are shown in Fig. 9, along with spectral analysis of signal and noise for the noise-reduced, rebalanced, velocity-converted iDAS data. We display uncorrelated data in true velocity units (nm/s); whereas for correlated data, following industry convention, we have normalized the correlated data. (Note that, for a sweep of amplitude A and length T the correlated amplitude is $A^2T/2$, but this is typically not removed as many sweeps are correlated with a synthetic pilot signal of arbitrary amplitude.) For our data, we have set the sweep autocorrelation equal to 1 and then divided by 3,500 m/s, yielding units for correlated data that are dimensionless nanostrain.

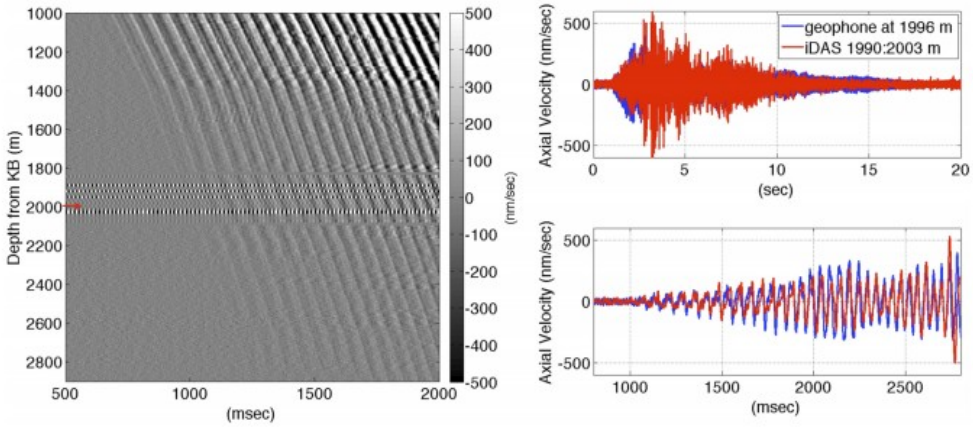

Figure 8 (A) SP 2021 DAS data uncorrelated, noise-reduced, rebalanced and velocity converted for a stack of 64 sweeps, shown with ~2 m channel spacing. In the zone covered by the geophone array (1,829 m to 2,088 m), the DAS data are overlain by geophone records. The geophone data have a stack of four sweeps, and the 60-Hz electrical noise from some geophones is easily seen. (B) (top right) A full 20 s of data for a single geophone at 1,996 m (blue) and the DAS data summed over a 13-m interval centred at the geophone. (C) (lower right) Same as (B) but with the data having a zoom view of 500 ms–3,000 ms. Note that the DAS and geophone data have been independently converted to true velocity units (nm/s) and only normalized by the number of sweeps.

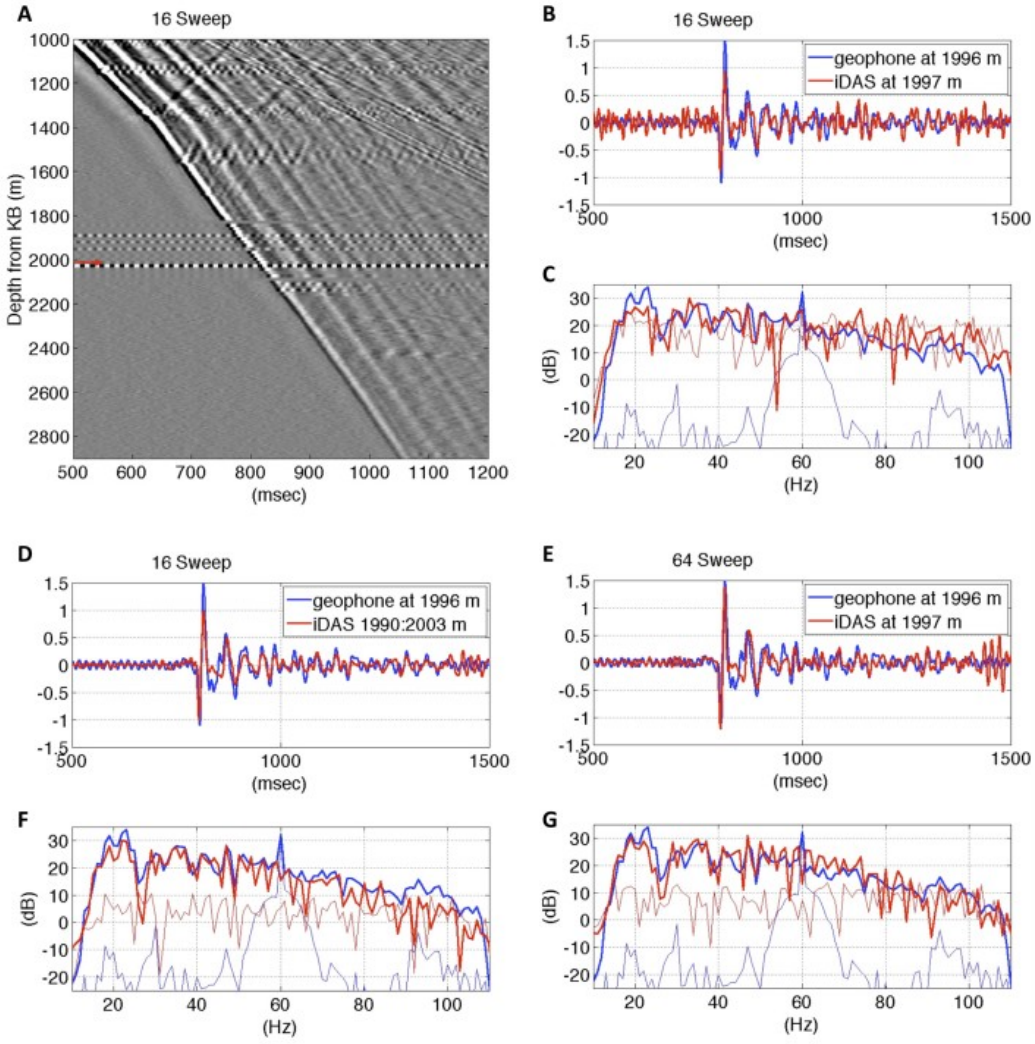

Figure 9 All panels show DAS data noise-reduced, rebalanced, and correlated with a normalized sweep. The geophone data is a stack of four sweeps and has been correlated with the same normalized sweep and then divided by 3,500 m/s to give comparable dimensionless nanostrain. Panels show DAS data with a stack of either 16 sweeps (A–D, F) or 64 sweeps (E, G), and correlated geophone data with a stack of four sweeps. (A) Comparison of about 1,900 m (950 channels) of DAS data with about 260 m (18 channels) of geophone data inserted at their depths. (B) Data for a single geophone at 1,996-m depth (indicated with red arrow in (A)) and the DAS data from the nearest channel (with centre at 1,997 m). (C) Spectra for DAS and geophone data of (B) for signal (dark lines) and noise (light lines). (D) and (E) show a comparison of single geophone to (D) DAS summed over a 14-m channel interval centred at the geophone and (E) data from the single nearest DAS channel. (F) and (G) show spectra for the data in (D) and (E), respectively. For the spectral plots, 'signal' in dark curves is calculated from data in a 500 ms–1,500 ms time window (peak seismic wave amplitudes), whereas 'noise' (light red and light blue curves) is from data in a time window of 8,000 ms–9,000 ms (after seismic waves have decayed to minimal amplitudes).

By calculating the mean RMS noise levels, we can quantitatively evaluate DAS SNR as a function of stacking fold. Using uncorrelated DAS data (after noise suppression, rebalancing, and multiplication by 3,500 m/s, the reference propagation velocity *c*), we calculated the noise level for each trace as the RMS amplitude in a 500-ms window (200 m–700 ms, before the arrival of the sweep) and then averaged the noise estimates of all traces in the depth interval of 2,000 m –2,800 m. In this interval, we find the following: a four-sweep stack has RMS noise of 186 nm/s, 16 sweeps have RMS noise of

89 nm/s, and 64 sweeps have RMS noise of 43 nm/s. This is about 6.4 dB for each factor of 4 in sweeps (with a ‘theoretical’ expectation of 6 dB).

Similarly, DAS noise is reduced by sampling larger spatial intervals via stacking of adjacent DAS channels. We find the decrease in mean RMS noise in the 16 sweep data, upon stacking every four channels, thus resampling from 2 m to 8 m output, is 5.5 dB (from 89 nm/s to 47 nm/s RMS), slightly lower than the theoretical 6 dB.

The data of Fig. 9, which compares a vertical geophone to DAS data converted to axial velocity, demonstrates a number of comparison observations.

The recovered DAS signal spectrum can match the recovered geophone signal spectrum, within the source bandwidth used at Citronelle (see Fig. 9C, F, and G).

With independent processing and nominal gains, there is a clear similarity of amplitude and phase response (i.e., the time series) between geophone and DAS (see Fig. 9B, D, and E).

DAS spatial sampling can be used to average over larger intervals to improve SNR. Improvements in the signal processing discussed above, along with a reasonable extra source effort, have enabled us to achieve time series and signal spectra that are similar to the geophone data using a portion (15 m) of the DAS data (see Fig. 9D and F). Alternatively, DAS data with finer spatial sampling (~2 m) can be made similar to geophone data (at a coarser sampling of 15 m) with greater extra source effort (See Fig. 9 E and G). Note that because the DAS data are averaging strain over the selected gauge length, the spatial sampling of DAS ‘channels’ is correctly comparable to geophones only when the signal wavelengths are large enough to be constant over a gauge length, whereas geophone data are spatially aliased if signal wavelengths are less than twice the geophone spacing.

The SNR comparison of DAS and geophone data is dominated by variability in the noise spectra. With reasonable stacking of sweeps or channels, we find the DAS SNR to be about 18 dB–24 dB below the geophone data outside of the 60-Hz noise band (see Figs. 9F and G). Within the 60-Hz noise band, the SNR is actually better for DAS. This result highlights an attribute of DAS seen in Fig. 9, which is the lack of sensitivity to electrical noise. The noise in the geophone data is dominated by 60 Hz (power line) electrical noise, most visible at depths where geophone wiring has electrical leakage to ground. Our numerical comparison of RMS noise levels between DAS and geophones depends on our choice of what geophone to use as “typical” (some were much noisier that the one we chose) and upon our choice to evaluate the geophone noise level without attempting to remove this narrow-band noise. In Fig. 9 (F, G), the relatively flat noise level in the DAS is about 25 dB higher than the best part of the geophone spectrum and about 25 dB lower than the worst part of the geophone spectrum (near 60 Hz).

We also have observed a difference in sensitivity to tube waves (borehole interface waves) such that the geophones, which are actively clamped to casing and decoupled from the tubing string, show reduced tube-wave sensitivity compared with the fibre cable in the flatpack, which is strapped continuously to the tubing (see event before the end of trace in Fig. 9E, about 1,450 ms–1,500 ms). While geophone clamping is known to reduce tube-wave sensitivity, the uncertain coupling of the fibre cable (described above) makes quantitative comparative analysis difficult. Clearly, coupling of the fibre cable should be actively considered in DAS survey design, just as geophone coupling is considered. As pointed out by Daley *et al*. (2013b), using the Citronelle DAS data, the observation of two distinct tube-wave speeds indicates a tube-wave coupling between the fluid-filled annulus and the central portion of the tubing.

6 VERTICAL SEISMIC PROFILE ANALYSIS

We can now compare data in the context of the goals of a typical vertical seismic profile (VSP) survey—imaging the subsurface. Imaging is improved with increasing spatial coverage and sampling. A primary attribute of distributed acoustic sensing (DAS) VSP data, as compared with traditional geophones, is large spatial coverage at small sampling intervals. Figure 7 demonstrated that the modular borehole monitoring (MBM) tubing-deployed fibre can obtain useful VSP data over nearly 3 km of borehole from a reasonable source effort (16 vibroseis sweeps). For comparison of DAS to the MBM geophones (18 sensors spaced ~15 m (50 ft) between 1,829-m and 2,088-m depth), the vertical geophone data is inserted in a DAS data plot (Fig. 9). Figure 9 shows both the match of data phase and signal-to-noise ratios (SNR) described above and the much greater spatial sampling achieved by DAS from a single source stack. While the MBM tubing deployment has many fewer sensors than a typical temporary wireline-deployment geophone VSP, semi-permanent geophone arrays are often limited to 10–20 levels as in the MBM.

Depth estimation

Both precision and accuracy in sensor depth are important for VSP analysis. DAS depths are measured via the speed of light in the fibre (e.g., Daley *et al*. 2013b). However, DAS data has inherent depth uncertainty due to extra fibre length (EFL) installed in the fibre encapsulation to prevent fibre breaking due to differential stretch of glass fibre and steel encapsulation. Additionally, the fibre cable inevitably has some spiraling on the tubing, whereas the tubing itself has some spiraling during deployment, both of which add length and reduce certainty with regard to the physical depth increment per channel. Therefore, the accuracy of the assigned depths depends upon knowing one or more physical locations where the corresponding DAS channel is confidently determined.

For Citronelle, we used two reference depths for calibration: the surface well head and the packer. The packer depth below surface was determined via

measurement of tubing joint lengths and its location relative to the fibre was confirmed with distributed temperature sensing (DTS) and heat-pulse analysis as 2,873 m. Previous use of the MBM for distributed heat-pulse studies (Daley *et al*. 2013a) had located wellbore completion components (such as the top of packer and the end of the flatpack) with a precision of about 0.25 m. The DTS system used in this study has higher spatial resolution than DAS (about 0.15 m) while still measuring the fibre length. By assigning the packer depth to the DAS channel observed to have tube-wave reflections coming from the packer, we fixed a deep DAS channel at a known depth. A shallow DAS channel was fixed by a 'tap test' on the wellhead (just above ground level). Dividing the depth difference with the number of channels, we were able to estimate the distance per channel and compare that result to the true fibre length from optical measurement. The result was an EFL of 0.74%, giving a DAS channel spacing of 2.033 m rather than the nominal (straight) length of 2.048 m. Similarly, the DAS data depth can be calibrated by matching observed DAS reflection depths with well-log measured property change, such as a reflection from a sonic velocity change at ~1,360 m. Thus, the complete sampling of the well with fine spacing allows the DAS data set to potentially address the problem of depth matching for DAS channels within the spatial resolution of the DAS system.

Deconvolution

A standard component of VSP processing is designing a deconvolution (decon) operator based on the downgoing wavefield (e.g., Hardage 1985). The fact that DAS VSP data will typically cover the entire well increases the precision of the downgoing decon operator design, leading to improved quality of deconvolved data. We have applied a downgoing decon based on (Haldorsen, Miller, and Walsh 1994). The overall quality of deconvolved DAS VSP data is shown in Fig. 10, which has nearly the entire ~2,900-m dataset. Comparing Fig. 7 (or 9a) with Fig. 10 shows the effect of the downgoing deconvolution in removing multiples. Note that the deconvolved wavelet is zero phase and, with the reduced DAS noise level, has visible side lobes before the first arrival.

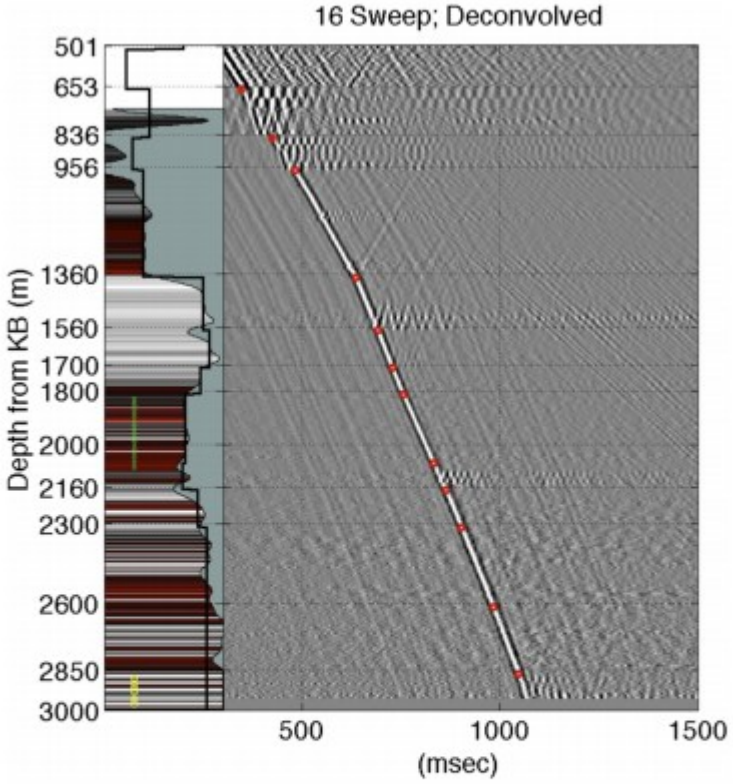

Figure 10 Deconvolved DAS data for a stack of 16 source sweeps. The far left panel, which is coloured by gamma-ray log data, shows local velocities and a blocked velocity model (thick black line) that were both derived from picked DAS first arrival times. Depths associated with major velocity changes in the DAS data are indicated with red dots.

Interesting features can be observed in Fig. 10. Notable are zones of ‘ringing’ (reverberant events trapped between two depths, such as a waveguide). We hypothesize that these events are related to waves propagating in the steel casing and may be related to a lack of cement bond at these locations. For example, between 653 m and 836 m, in Fig. 10, the waves can be seen to have initial downgoing segment with faster apparent velocity than the P-wave, indicating propagation at least partly in non-formation material (likely steel or cement). Another feature demonstrated in Fig. 10 is the depth match between well-log measured interfaces and the reflected events observed in the VSP, e.g., the reflection event at 1,360 m.

Vertical seismic profile reflections

Following conventional VSP processing, including deconvolution, the DAS data can provide upgoing reflectivity, which is typically one primary goal of a VSP survey. The processing for reflections included the following operations: deconvolution, time shifting to two-way travel time, smoothing with a temporal 10–110 Hz bandpass and a running 300-m median filter. These

operations were applied to both DAS and MBM geophone data, and the results are compared in Fig. 11. Increased coherence of reflections is observed in the DAS data. Also shown in Fig. 11 is a corridor stack (Hardage 1985) and well-log data. Increased vertical extent of DAS reflection data, above the geophones, is seen by comparing the two corridor stacks in Fig. 11.

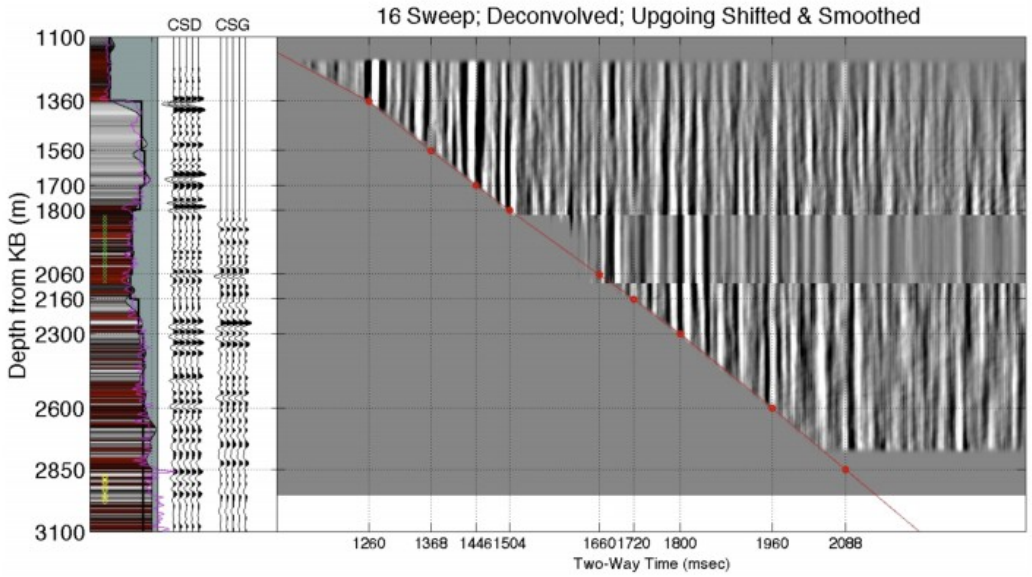

Figure 11 Upgoing reflections from DAS VSP (right) with MBM geophone data inserted, along with corridor stacks for both DAS (labelled CSD) and geophones (labelled CSG). The far left panel that is coloured by gamma-ray log data shows local velocities and a blocked velocity model that were both derived from picked DAS first arrival times. A smoothed sonic log is plotted in magenta using measured slowness smoothed by filtering with a tapered 15-m averaging window. The reflection panel shows depths associated with major velocity changes in DAS data indicated by red dots and DAS picked travel times (red line).

7 SUMMARY AND CONCLUSIONS

A modular borehole monitoring (MBM) system was designed and successfully deployed in a 2,900-m well for CO_2 monitoring. The tubing-deployed MBM system provided a platform for simultaneous acquisition of clamped geophone and distributed acoustic sensing (DAS) vertical seismic profile (VSP) data, allowing direct comparison of two sensor types. Excellent VSP results were obtained from three test source points. Improvement in DAS data quality from the initial 2012 test shown by Daley *et al*. (2013) was clear and unambiguous. Improvement was seen initially due to improved recording procedures and DAS acquisition hardware. Further improvement was gained from DAS processing.

We have described the native measurement in the iDAS unit as localized strain rate. Following a processing flow of adaptive noise reduction and rebalancing the signal to dimensionless strain, standard improvement from repeated stacking of the source was observed (i.e., the remaining DAS noise is temporally flat and uniform between channels while the signal is repeatable). Conversion of the rebalanced signal to equivalent velocity units allows direct comparison of DAS and geophone data. We obtain a very good

match of uncorrelated time series in both amplitude and phase, demonstrating that velocity-converted DAS data can be analysed equivalent to vertical geophones. Comparison of signal-to-noise ratios (SNRs) between distributed sensors and point sensors (i.e., DAS and geophones) can be done in various ways. For a single DAS channel (2-m spacing with a 10-m gauge length), we find a time series comparable to the MBM geophone was obtained with about 16 times the source effort (4 versus 64 sweeps), implying about 24 dB greater sensitivity for the casing-clamped geophone than the tubing-clamped fibre in flatpack. However, with stacking of channels for a 15-m section of the DAS cable (the distance between geophones) centred at a geophone, a comparable time series is obtained with about four times the source effort (4 versus 16 sweeps), or about 12 dB greater sensitivity for the clamped geophone. Comparison of spectral SNR is dominated by spectral variability, mainly due to electrical noise on the geophone data in the 50 Hz–70 Hz band. In general, we find the DAS data SNR to be 18 dB–24 dB below the MBM geophone data. These are key conclusions of our test.

The DAS recordings were processed for VSP reflectivity, including downgoing wavefield deconvolution and generation of corridor stacks, both of which are improved by the fibre cable's large spatial coverage. This is an advantage of DAS over geophone arrays with limited length (such as the Citronelle MBM array). Following depth corrections, the reflectivity was shown to have very good correlation to intervals interpreted from well log data. The DAS recordings also appear sensitive to well completion, with zones of trapped energy interpreted as related to casing bond. This observation requires further dedicated study and has potential use for wellbore integrity studies.

We have described many fundamental attributes of DAS VSP data and compared data quality of tubing-coupled fibre cable to casing-clamped geophones. During testing at the Citronelle site, we have seen improvement in the specific DAS recording system used (the iDAS) and expect further improvements to iDAS technology. An important observation is that the cost and effort of the clamped geophone deployment was far more than the fibre cable deployment. Therefore, the extra seismic source effort currently needed for tubing-deployed DAS seems to be well compensated by the benefit of extra spatial sampling and lower deployment cost. Further study and improvement in DAS technology and deployment should lead to further gains in a cost-to-benefit ratio. For the application of long-term seismic monitoring of carbon sequestration, as well as other applications, DAS VSP appears to be a useful and promising tool.

8 ACKNOWLEDGEMENTS

We would like to thank the CO2 Capture Project for support of the modular borehole monitoring (MBM) concept, development, and deployment. We thank the SECARB team, including Jerry Hill of SSEB, Rob Trautz of EPRI, George Koperna and Dave Riestenberg of ARI, and Gary Dittmar of Denbury.

Acquisition of seismic data (geophone and DAS) was assisted by Dale Adessi of SR2020 and Michelle Robertson of LBNL. We would like to thank Bjorn Paulsson and John Thornburg of Paulsson, Inc. for the fabrication and deployment support of MBM geophones. This paper was greatly improved by the efforts of the anonymous reviewers and the editor. This work was supported by the CO_2 Capture Project, and performed by Lawrence Berkeley Laboratory under Contract No. DE-AC02-05CH11231.

APPENDIX A

In this appendix, we describe in more detail the adaptive stacking discussed above. For illustration, Figure A-1(a) (upper) shows a 2.5-s window of native-format output from the iDAS channel at 1,996 m for an early time window (0.5 to 3 s) of 64 consecutive sweeps. To good approximation, this is the sum of common signal plus broadband noise, which is incoherent with respect to both signal and sweep number. The noise amplitude is highly skewed and randomly located in time, with a few very noisy sections accounting for most of the noise energy. Within individual traces, the noise amplitude drifts slowly with time.

Figure A1(b) (middle) shows the stacking (both simple and adaptive) and rebalancing result for the 64 time series in A-1(a). In this figure, the uncorrelated sweep can be seen emerging between 1.5 s and 3.0 s, most clearly in the weighted-averaged rebalanced (WAR) data.

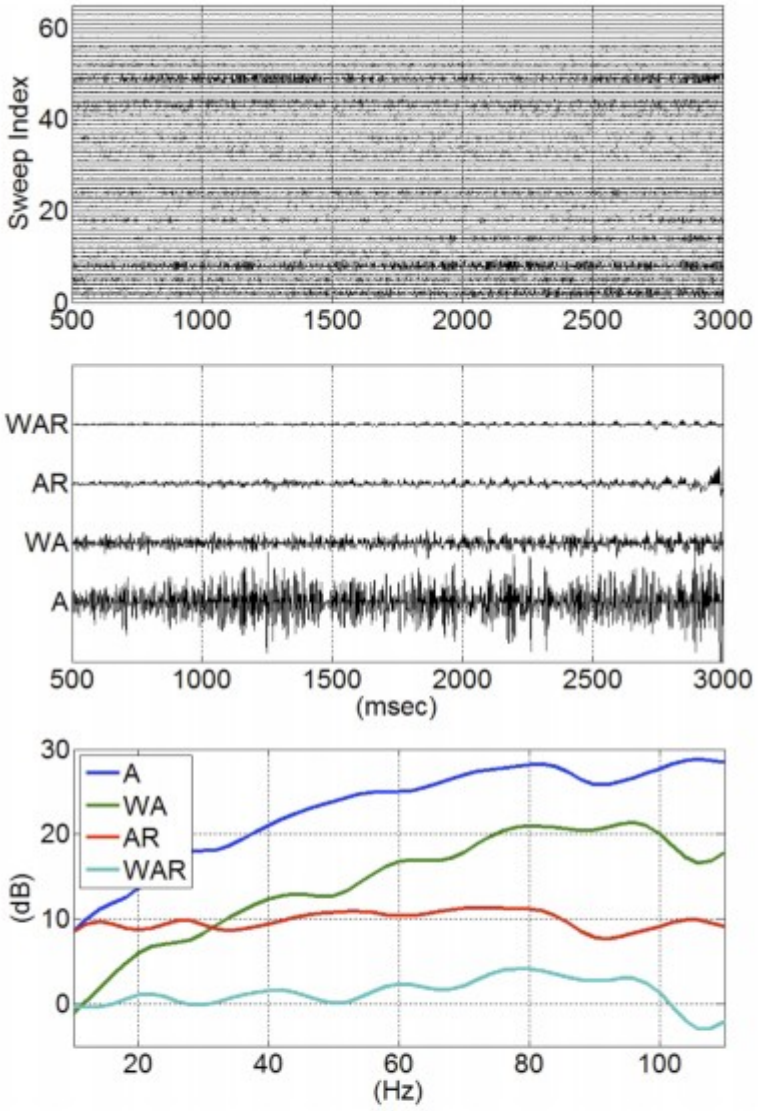

Figure A1 (a) (upper panel) Native-format output (strain rate) time series from the iDAS channel at 1,996 m for 64 consecutive sweeps. (b) (middle panel) Comparison of simple and adaptive stacking before and after rebalancing. (c) (lower panel) Comparison of spectral power estimates from the data in the middle panel. In (b) and (c), A is a simple average; WA is a weighted average derived from the proprietary noise-power estimate; AR is the result of applying the spectral rebalancing to the simple average; and WAR is the result of applying the spectral rebalancing to the optimally weighted average.

Figure A1 (lower) compares spectral power estimates from the data in the upper panel. The spectra were obtained by applying a 20-Hz smoothing filter to power spectra calculated by Fourier transform of the window from 200 ms to 700 ms, which represents pure noise before the arrival of first signal. After

rebalancing, the traces have units of dimensionless strain. For the rebalanced traces in this noise window, the RMS noise level for AR is 43.8 pico-strain (43.8e-12), whereas WAR is 16.6e-12. Corresponding velocity values can be obtained by multiplying by a representative propagation speed. Thus, for example, the WAR noise level has an equivalent value of 58.1e-9 m/s with respect to propagation at 3,500 m/s.

Adaptive Stacking

To good approximation, repeat iDAS shots and/or recordings from very closely spaced channels satisfy three assumptions:

(i) Signal is constant from trace to trace and uncorrelated with noise.

(ii) Noise on individual traces is broadband, zero-mean, incoherent and uncorrelated from trace to trace.

(iii) Noise power is variable from trace to trace but slowly varying within any trace.

Under these assumptions, a weighted mean stack can have significantly higher SNR than a simple mean stack. Optimal stacking weights can be obtained as follows (cf. Embree 1968).

Given an array of recorded data traces $d_i(t)$, i = 1, ... M satisfying assumptions (i)-(iii) above, and a set of slowly time-variant weighting coefficients $w_i(t)$, i = 1, ... M satisfying *for all t*

$$\sum_{i=1}^{M} w_i(t) = 1, \quad \text{(A1)}$$

it follows from (i)-(iii) that to good approximation, the weighted mean

$$D(t) = \sum_{i=1}^{M} w_i(t)\ d_i(t) = \sum_{i=1}^{M} w_i(t)\ (S(t) + n_i(t)), \quad \text{(A2)}$$

satisfies

$$D(t)^2 = S(t)^2 + \sum_{i=1}^{M} w_i(t)^2 n_i(t)^2, \quad \text{(A3)}$$

where *S(t)* is the common signal and $n_i(t)$ is the noise in the *i*th trace. Note that we have dropped a cross term based on the assumption that the noise is zero-mean and uncorrelated with the signal.

Thus to good approximation the SNR of the weighted mean is maximized by finding a weighting vector *w(t)* that minimizes the noise power

$$\mathcal{N}(\mathbf{w}(t)) = \sum_{i=1}^{M} w_i(t)^2 n_i(t)^2, \quad \text{(A4)}$$

subject to the constraint A1.

This problem is solved by the method of Lagrange multipliers (e.g. O'Neil, 1975, section 5.9). For notational clarity, we drop the explicit reference to

time, but it should be understood that all quantities may vary as a function of time.

We form the Lagrange function

$$\mathcal{L}(\boldsymbol{w}, \lambda) = \mathcal{N}(\boldsymbol{w}) + \lambda \left(\sum_{i-1}^{M} w_i - 1 \right), \quad \text{(A5)}$$

then solve

$$\nabla_{\boldsymbol{w},\lambda} \mathcal{L} = 0, \quad \text{(A7)}$$

for *w* and λ. Asserting A7,

$$\frac{\partial \mathcal{L}}{\partial \lambda} = 0, \quad \text{(A8)}$$

is equivalent to A1 and

$$\frac{\partial \mathcal{L}}{\partial w_i} = 0, \quad \text{(A8)}$$

yields

$$2\, w_i n_i^2 + \lambda = 0, \quad \text{(A9)}$$

hence

$$w_i = \frac{-\lambda}{2\, n_i^2}. \quad \text{(A10)}$$

Summing A10 over *i* and applying the constraint A1

$$1 = -\frac{\lambda}{2} \sum_{i-1}^{M} 1/n_i^2, \quad \text{(A11)}$$

hence

$$\frac{-\lambda}{2} = 1 \Big/ \sum_{i-1}^{M} 1/n_i^2, \quad \text{(A12)}$$

and, substituting into A10

$$w_i = \left(\frac{1}{n_i^2} \right) \Big/ \sum_{i-1}^{M} 1/n_i^2. \quad \text{(A13)}$$

Write

$$N_i = \left(\frac{1}{n_i^2} \right) \text{ and } \mathbb{N}^M = \sum\nolimits_{i-1}^{M} N_i. \quad \text{(A14)}$$

Then A13 becomes

$$w_i = N_i / \mathbb{N}^M. \quad \text{(A15)}$$

We observe

$$\mathcal{N}(\boldsymbol{w}) = \sum_{i-1}^{M} w_i^2\, n_i^2 = \sum_{1}^{M} \frac{\left(N_i / \mathbb{N}^M \right)^2}{N_i} = 1/\mathbb{N}^M, \quad \text{(A16)}$$

which may be recognized as 1/M times the harmonic mean of the noise power of the individual traces.

In practice, this reduces the problem of determining optimal stacking weights to the problem of estimating noise power.

Note that, for a fixed stacking fold, the improvement of the adaptive stack with respect to a simple mean depends on the difference between the arithmetic and harmonic means of the noise power. This, in turn, depends upon the skewness of the noise power distribution. For our rebalanced data in Fig. A1, that improvement is 20×log10(43.8/16.6) = 8.4 dB.

Equation A16 predicts the same scaling with stacking fold (3 dB per doubling of fold) for the adaptive stack as for the simple mean stack. As noted in our discussion of Fig. 9, we found a slightly higher rate of improvement with stacking fold (6.4 dB per factor of four in fold) for our data.

REFERENCES

Aki K. and Richards P.G. 2002. *Quantitative Seismology*. University Science Books, pp. 635. Sausalito, CA.

CO2 Capture Project. 2009. *A Technical Basis For Carbon Dioxide Storage, CO2 Capture Project* [Online]. CPL Press ISBN 978-1-872691-48-0.

Daley T.M., Freifeld B.M., Cook P., Trautz R. and Dodds K. 2013a. Design and deployment of a modular borehole monitoring system at SECARB's Citronelle Sequestration Site. In: *12th Annual Conference on Carbon Capture, Utilization & Sequestration, Pittsburgh, Pennsylvania, 13 – 16, May 2013*.

Daley T. M., Freifield B.M., Ajo-Franklin J., Dou S., Pevzner R., Shulakova V. *et al*. 2013b. Field testing of fibre-optic distributed acoustic sensing (DAS) for subsurface seismic monitoring. *The Leading Edge* 32(6), 699– 706.

Embree P. 1968. *Diversity Seismic Record Stacking Method and System. U.S. Patent 3398396 A*.

Esposito R., Rhudy R., Trautz R., Koprena G., and Hill G. 2011. Integrating carbon capture with transportation and storage, *Energy Procedia* 4, 5512–5519.

Farhadiroushan M., Parker T.R. and Shatalin S. 2009. *Method And Apparatus For Optical Sensing*. WO2010136810A2.

Freifeld B.M., Daley T.M., Hovorka S.D., Henninges J., Underschultz J. and Sharm S. 2009. Recent advances in well-based monitoring of CO_2 sequestration. *Energy Procedia* 1, 2277– 2284.

Haldorsen J.B.U., Miller D.E. and Walsh J.J. 1994, Multichannel Wiener deconvolution of vertical seismic profiles. *Geophysics* 59(10), 1500– 1511.

Hartog A., Kotov O.I. and Liokumovich L. 2013. The optics of distributed vibration sensing. In: *Second EAGE Workshop on Permanent Reservoir*

Monitoring 2013 – Current and Future Trends, Stavanger, Norway, 2–5 July 2013.

IPCC. 2005. *IPCC Special Report on Carbon Dioxide Capture and Storage. Prepared by Working Group III of the Intergovernmental Panel on Climate Change* (eds. B. Metz, O. Davidson, H.C. Coninck, M. Loos, and L. A. Meyer), pp. 442. Cambridge University Press, Cambridge, United Kingdom and New York, NY, USA.

Mateeva A., Mestayer J., Cox B., Kiyashchenko D., Wills P., Lopez J. *et al*. 2012. Advances in distributed acoustic sensing (DAS) for VSP. 2012 SEG meeting, Las Vegas, USA, Extended Abstract.

Mateeva A., Lopez J., Potters H., Mestayer J., Cox B., Kiyashchenko D. *et al*. 2014. Distributed acoustic sensing for reservoir monitoring with vertical seismic profiling. *Geophysical Prospecting* 62, 679– 692.

Mestayer J., Grandi Karam S., Cox B., Wills P., Mateeva A., Lopez J. *et al*. Distributed acoustic sensing for geophysical monitoring. 74th EAGE Conference & Exhibition incorporating SPE EUROPEC 2012 Copenhagen, Denmark, 4–7 June 2012.

Miller D., Parker T., Kashikar S., Todorov M., and Bostick T. 2012. Vertical seismic profiling using a fibre-optic cable as a distributed acoustic sensor. 74th EAGE Conference & Exhibition incorporating SPE EUROPEC 2012 Copenhagen, Denmark, 4–7 June 2012.

O'Neil P.V. 1975. *Advanced Calculus, Pure and Applied*. Macmillan, New York. ISBN 0-02-389320-6.

Parker T., Shatalin S. and Farhadiroushan M. 2014. Distributed acoustic sensing – a new tool for seismic applications. *First Break* 32(2), 51– 69.

Riestenberg D. 2012. SECARB Citronelle geologic characterization. SECARB Joint Project Review Meeting, June 14, 2012.

SECARB. 2012. *Southeast Regional Carbon Sequestration Partnership Phase III Anthropogenic CO2 Injection Field Test*, http://www.secarbon.org/files/anthropogenic-test.pdf, accessed March 2014.

Widrow B., Glover Jr. J.R., McCool J.M., Kaunitz J., Williams C.S., Hearn R.H. *et al*. 1975. Adaptive noise cancelling: principles and applications. *Proceedings of the IEEE* 63(12), 1692.